*Article*

# Failure Assessment of Steel/CFRP Double Strap Joints

**Hamid Reza Majidi [1], Seyed Mohammad Javad Razavi [2] (ID) and Filippo Berto [2,\*]**

[1] Department of Mechanical Engineering, Iran University of Science and Technology, Narmak, Tehran 16846, Iran; hr.majidi_mech@yahoo.com
[2] Department of Mechanical and Industrial Engineering, Norwegian University of Science and Technology (NTNU), Richard Birkelands vei 2b, 7491 Trondheim, Norway; javad.razavi@ntnu.no
\* Correspondence: filippo.berto@ntnu.no; Tel.: +47-7359-4129

**Abstract:** In the current study, the failure behavior of retrofitted steel structures was studied experimentally and theoretically with steel/carbon fiber reinforced polymer (CFRP) double strap joints (DSJs) under quasi-static tensile loading. A series of DSJs with different bonding lengths are also considered and examined to experimentally assess the effective bond length. To predict the failure load values of the tested specimens, a new stress-based method, namely the point stress (PS) method is proposed. Although some theoretical predictive modelling for the strength between steel/CFRP joints under various loading conditions has been presented, in this work by using the new proposed approach, one can calculate rapidly and conveniently the failure loads of the steel/CFRP specimens. Furthermore, to assess the validity of the new proposed method, further experimental data on steel/CFRP DSJs available in the open literature are predicted using the PS method. Finally, it was found that a good agreement exists between the experimental results and the theoretical predictions based on the PS method.

## 1. Introduction

Nowadays, application of adhesively bonded joints in steel structures instead of conventional mechanical fastening methods like bolting or welding often offers by engineers because of the reduced weight and cost. In recent decades, carbon fiber reinforced polymer (CFRP) laminates have been widely used in various industries such as aerospace, marine, wind energy structures, etc. One of the major applications of CFRP patches is to retrofit the damaged steel structures and also reduction of the overall weight of structure. For example, in Boeing 787 aircraft, 43% of metal structures were replaced by CFRP laminates such as fuselage, wing, etc. [1]. Therefore, a suitable failure predictive approach to design the steel/composite bonded joints is necessary.

Although failure models in adhesively bonded structures are often presented in terms of the peel or shear stresses along the adhesive layer [2], some approaches based on fracture mechanics were proposed [3,4]. Therefore, to justify the present investigation a brief summary of some well-known failure criteria is given below to predict failure behavior for the adhesive joints.

Martiny et al., have evaluated the values of failure loads in metal-to-metal adhesive joints by means of a criterion based on attaining a critical value of the maximum principal stress at a critical distance ahead of the crack tip [5]. In the other investigations, the shear strain distribution along the adhesive mid-plane as the key parameter was considered to predict the failure load (see Refs. [6–8]). Recently, some researchers have investigated the failure behavior of metal fiber-reinforced adhesive joints by considering the shear and peel stress distributions along the adhesive mid-plane [9–11].

For the cases in which the plastic deformation occurred in the adhesive layer, Hart-Smith [12] proposed the maximum shear strain as a failure criterion. More recently, da Silva et al. [13,14] have indicated that the maximum shear strain criterion is very accurate for single lap joints with ductile adhesives. Also, a shear stress approach has been extensively utilized to predict the strength of the lap joint. John et al. [15] used the shear stress method by considering the specified critical distance in their numerical calculations to predict the ultimate failure of double lap joints. Moreover, the maximum shear stress has been applied in tubular joints to estimate their failure behavior by Adams and Peppiatt [16] and Lee and Lee [17]. da Silva et al. [13,14] utilized this criterion to predict the failure of the single lap joints and finally they have concluded that this approach is verified by the experimental data only in the case of brittle adhesives and short overlaps. In another paper, by using an energy-based failure criterion, the crack propagation process and failure load of the adhesive lap joints have been predicted by Chen et al. [18].

The double strap joint (DSJ) as a well-known experimental specimen is extensively used to investigate the strength of steel/composite joints. Failure mechanisms in damaged steel structures which have been repaired or reinforced with CFRP patches have been assessed by various failure criteria. In the following, some of the researches dealing with DSJs especially steel/CFRP bonded joints which were recently published in open literature are mentioned briefly. Chalkley and Rose [19] have investigated theoretically the double-strap joints by means of stress analysis based on a modification of Hashin's variational method for orthogonally cracked composite laminates. Bocciarelli and co-researchers [20] analytically investigated the debonding strength behavior of steel/CFRP joints under tensile loading by using the stress-based criteria. Finally, they have shown that the results of stress-based criterion are in good agreement with the experimental results [20]. The influences of various geometrical and environmental parameters on the joint strength of steel/CFRP DSJs were studied by some researchers (see for instance Refs. [21–32]).

Fawzia et al. [22] tested the steel/CFRP DSJs by applying the wet lay-up method. They studied four variable parameters in their experiments such as: CFRP bond lengths, adhesive layer thickness, different types of adhesives, and adhesive maximum strain [22]. Nguyen et al. [25] have examined a series of DSJs with different bonding lengths which were tested at temperatures between 20 and 60 °C. They studied the mechanical characteristics such as strength degradation, stiffness, and change of effective bond length for steel/CFRP bonded joints at elevated temperatures [25]. Additionally, these experimental failure load results have been successfully predicted by the Hart-Smith model [25]. Al-Mosawe and co-researchers [30] have investigated the effect of CFRP properties on the bond characteristics in steel/CFRP DSJs under quasi-static loading. They conducted three-dimensional analyses considering non-linear behavior of the materials to study the effect of CFRP properties on the strain distribution and adhesive joint strength of the DSJ specimens [30]. In the other work, the bond behavior between CFRP patches and steel substrates under different loading rates have been studied by Al-Mosawe et al. [31]. Their results showed that, although the high loading rates have little influence on the effective bond length, these specimens experienced enhancement in the bond strength under impact loading by increasing the loading rates [31]. Al-Zubaidy et al. [26] have investigated the effect of loading rate for bond strength of DSJs, experimentally. In the other separate research [28]; they have predicted the results of failure load of the tested specimens in Ref. [26] by using the numerical prediction based on the cohesive zone model (CZM). Additionally, Zhao and Zhang have reviewed research in which the bond strength and fatigue crack propagation have been studied for steel/fiber reinforced polymers (FRP) components [33]. Also, more recently, Mohee et al. [34] has investigated failure modes, strength, design parameters, and performance of the steel/CFRP joints.

In this paper, a series of steel/CFRP DSJs were experimentally examined to assess their failure behavior. In fact, the aim of this research paper is to predict the failure loads of experimentally tested joints using the new failure predictive model, namely the point stress (PS) method. Furthermore, the PS method could predict successfully the experimental result of steel/CFRP DSJs under quasi-static

tensile loading. Further validations were undertaken using two series of experimental data available in literature.

## 2. Experimental Testing

DSJs made of two steel sheets (grades 300) and one unidirectional normal modulus CFRP ply on each side of the joints were fabricated with different bonding lengths. Figure 1 illustrates the schematic geometry of the test samples. The two components UHU® plus endfest 300 adhesive (UHU, Buehl, Germany) with weight mixing ratio of 100:50 for binder and hardener was used for bonding the adherends. The length, width and thickness of steel adherends were $L_{sub}$ = 200 mm, $B$ = 50 mm, $t_{sub}$ = 3 mm, respectively. Each layer of CFRP had a thickness of 0.176 mm, while the thickness of the adhesive layer was 0.5 mm. Separate standard tests were conducted on the steel plates (ASTM E8) [35] and adhesive material (ASTM D638) [36] in order to obtain the mechanical properties under tensile loading (see Table 1). The bonding length $L_1$ was always kept less than $L_2$ ($L_2 = L_1 + 30$ mm) to ensure that the failure occurred on the $L_1$ side only.

The steel plates were polished using a 240-grit sandpaper (Arsaco, Tehran, Iran) to increase the mechanical locking between the adhesive and adherends. Then, the polished surfaces were cleaned using cotton fabrics and acetone solution to remove dust and oil from the surface. After supplying the adhesive, DSJs were cured for 45 min at 70 °C and post-cured for 7 days at room temperature (about 25 °C). It is worth mentioning that the CFRP plies were co-cured with the DSJs. Different bonding lengths of $L_1$ = 10, 20, 30, 40, 50 mm were considered for experiments. For each geometry, at least four test samples were fabricated and tested using the universal tensile testing machine Instron ElectroPulsTM E10000 (Instron, Norwood, MA, United States) under quasi-static loading with a constant displacement rate of 2 mm/min, and the load–displacement curves of the joints were obtained. All the experiments were conducted at room temperature (25 °C) and relative humidity of 70%. Typical steel/CFRP DSJs before and after the tensile tests are shown in Figure 2. According to the test results, the DSJs with lower bonding lengths demonstrated a combined failure mode of CFRP rupture, CFRP delamination, and debonding between the CFRP and the adhesive layer. While, for DSJs with higher bonding lengths, the overall failure was governed by CFRP rupture and CFRP delamination. It is worth mentioning that as a result of a smaller required force of debonding between CFRP sheets and adhesive layer, lower failure loads were obtained for DSJs with shorter bonding lengths. A sample load–displacement curve of the tested steel/CFRP DSJs is depicted in Figure 3. Also, Table 2 presents details of each test including the dimensions of DSJs and the corresponding failure loads.
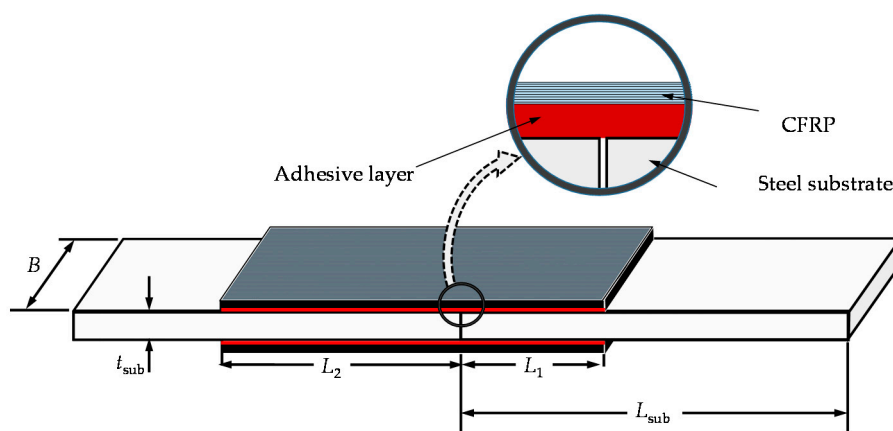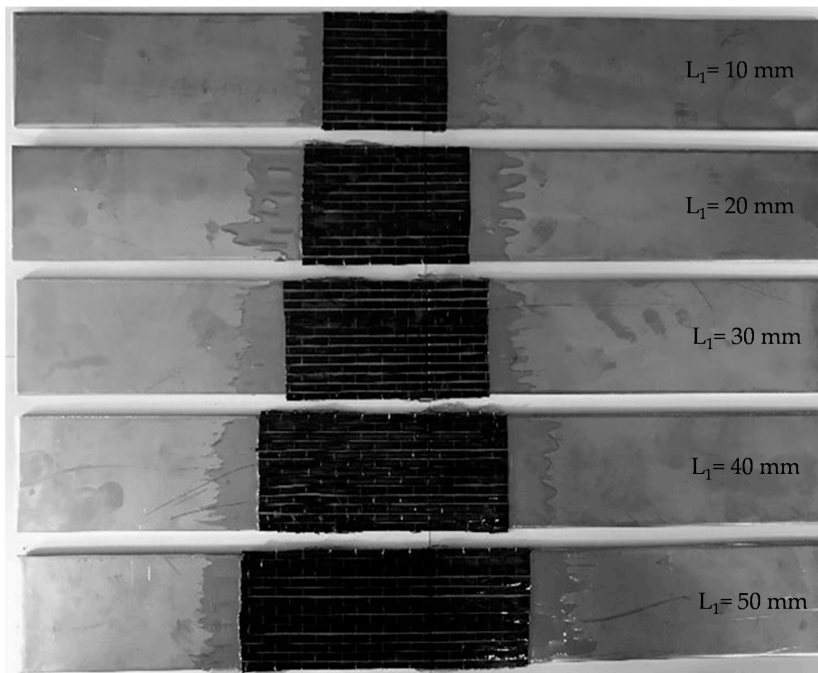


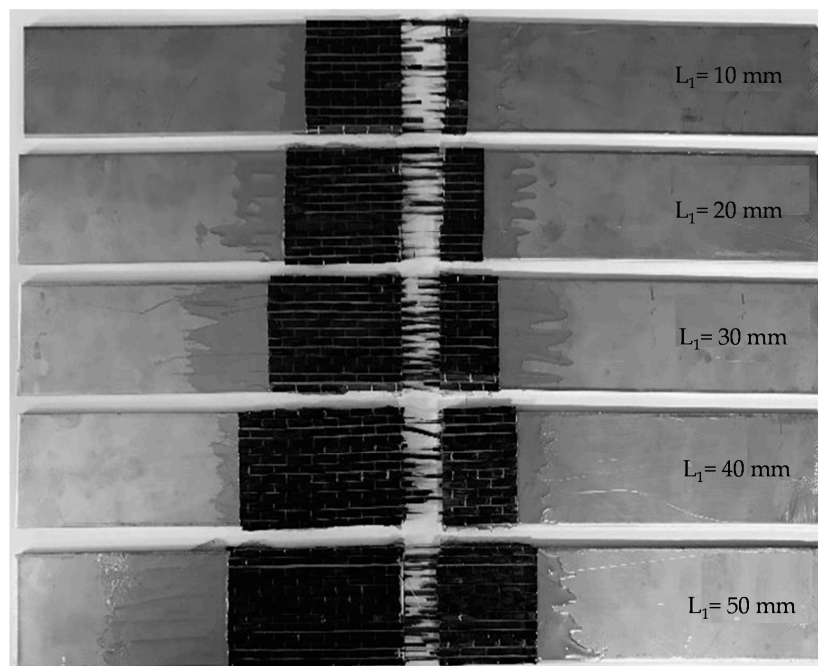**Figure 1.** A schematic of steel/CFRP double strap joint.

**Table 1.** Mechanical properties of materials used for experiments.

| Property | Steel Plates | Adhesive | CFRP Sheets * |
|---|---|---|---|
| Tensile modulus (GPa) | 203 | 2.1 | 200 |
| Poisson's ratio | 0.25 | 0.35 | 0.28 |
| Ultimate strength (MPa) | 520 | 39 | 1900 |
| Ultimate Strain (mm/mm) | 22 | 2.9 | 1.1 |

* Manufacturer's data.



(**a**)



(**b**)

**Figure 2.** Double strap joints (DSJs) prepared for experiments (**a**) before the test; (**b**) after the test.

**Table 2.** Details of experimental failure loads for the tested double strap joints (DSJs).

| Bonding Length, $L_1$ (mm) | Bonding Length, $L_2$ (mm) | Experimental Failure Load $P_{exp}$ (kN) |
|---|---|---|
| 10 | 40 | 14.80 |
| | | 13.19 |
| | | 11.86 |
| | | 13.47 |
| | | Average (Standard Deviation) = 13.33 (9%) |
| 20 | 50 | 23.21 |
| | | 26.57 |
| | | 22.24 |
| | | 25.42 |
| | | Average (Standard Deviation) = 24.36 (8%) |
| 30 | 60 | 32.89 |
| | | 33.12 |
| | | 30.98 |
| | | 28.73 |
| | | Average (Standard Deviation) = 31.43 (6%) |
| 40 | 70 | 31.58 |
| | | 28.25 |
| | | 31.15 |
| | | 29.70 |
| | | Average (Standard Deviation) = 30.17 (5%) |
| 50 | 80 | 31.45 |
| | | 30.41 |
| | | 33.22 |
| | | 32.64 |
| | | Average (Standard Deviation) = 31.93 (4%) |
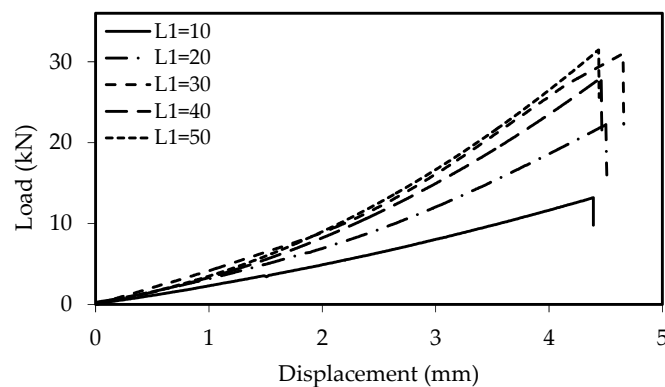


**Figure 3.** A sample load–displacement curve for the steel/CFRP DSJs under tensile quasi-static loading.

## 3. Finite Element Analysis

In order to predict the failure loads of DSJs, finite element analyses should be performed on DSJs to achieve the stress distribution across the adhesive mid-plane in the 2D model of specimens. According to the symmetry of the joints, only one quarter of the specimens were modeled (see Figure 4). The finite element program Dassault System ABAQUS-CAE-6.13 (NTNU, Trondheim, Norway) is utilized to study the finite element analyses for the DSJs. For this purpose, the CPE8R element type is used. This is an eight-node, biquadratic plane strain quadrilateral element with reduced integration. The boundary conditions and the applied loading to the finite element models are shown in Figure 4. The eight-node biquadratic plane strain quadrilateral elements with reduced integration were used for finite element simulation of adhesive joints. In order to ensure that the proper size of elements was used for analyses, a mesh convergence study was undertaken. Smaller elements were used in the adhesive layer to improve the accuracy of the output results. A typical mesh pattern used for

modelling DSJs is shown in Figure 5. This paper aims to evaluate the failure of DSJs using the elastic behavior of the joints. Also, as seen in Figure 2, the load–displacement curve is linear up to final fracture that takes place suddenly with no effective plastic deformation in the adhesive layer. Therefore, it is expected that the linear elastic assumption can be utilized for failure load prediction of the tested DSJs. For most of the structural adhesives which behave predominantly in a linear manner until the final failure, an assumption of linear elastic behavior is appropriate. Therefore, the non-linear geometry is not considered in the finite element (FE) simulations.
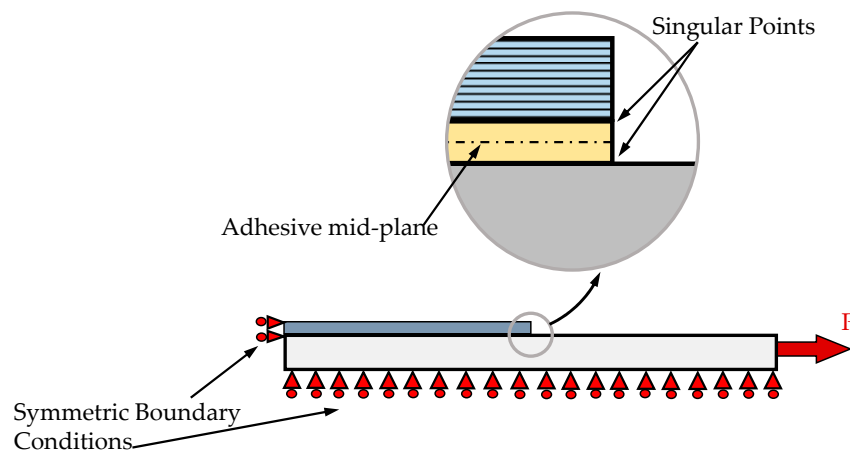


**Figure 4.** The applied boundary and loading conditions to the finite element model. (*P*: applied load)
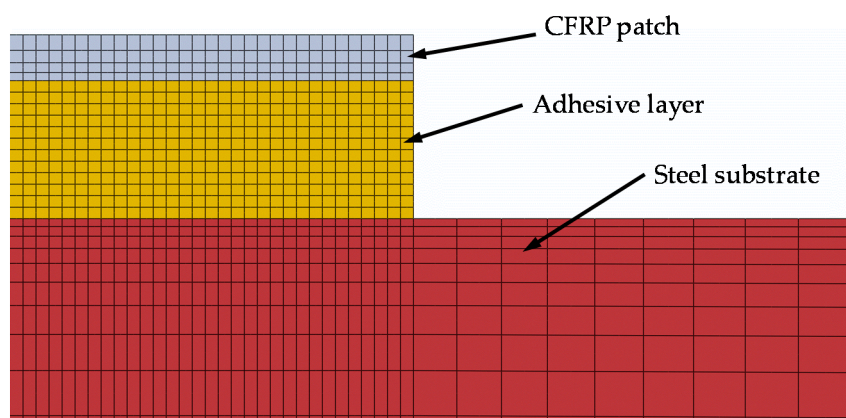


**Figure 5.** A typical mesh pattern used for DSJ models.

## 4. Failure Load Prediction

In this section, a stress-based method is presented to obtain the effective bond length and predict the load-bearing capacity of adhesively bonded DSJs. As an important parameter, the effective bonding length of DSJs should be calculated before failure load predictions using the PS method. According to the experimental results and also other available data in the literature related to adhesive joints, increasing the bonding length of adhesive joint results in higher load bearing capacity of the joint. However, for the adhesive joints with the bonding lengths higher than a specific value, the failure load would remain the same. This specific bonding length is named the effective bonding length, $L_{\text{eff}}$.

In this paper, a simple method is proposed to obtain $L_{\text{eff}}$ using 2D linear elastic finite element analysis. Unlike the previously proposed failure model, this methodology only requires elastic modulus and Poisson's ratio for calculating the effective bonding length. For this aim, finite element models of DSJs with different bonding lengths should be analyzed under a constant statically applied stress. One of the DSJs with a specific bonding length should be considered as the reference

joint. The longitudinal stress variation along the adhesive mid-plane should be exported, and then the value of the first pick in longitudinal stress curve should be recorded as critical stress $\sigma_{cr}$. The corresponding critical longitudinal stress values in the rest of the joints should be obtained. Comparing the critical longitudinal stress values for different bonding lengths reveal the effective bonding length. For the DSJs with the bond length higher than the effective bond length, the critical longitudinal stress remains constant. In the next subsection, the PS method is described to directly determine the value of the effective bond length before performing any experiments.

### 4.1. How to Calculate the Effective Bond Length by Applying the Point Stress (PS) Method

Here, the joint with 10 mm bonding length was selected as the reference joint. An axial tensile stress equal to 1000 MPa was applied to the joint and the variation of longitudinal stress along the adhesive layer was obtained. The first positive pick stress from the bond line edge was considered as critical longitudinal stress $\sigma_{cr}$ and it was equal to 8.62 MPa for the joint with 10 mm bond length. The key parameter in a failure method must be consistent with the detected failure mechanism in the tested joints. According to the CFRP rupture and delamination failure mechanisms, which are due to the longitudinal stress at the junction of steel adherends, longitudinal stress along the adhesive mid-plane was considered as the key parameter in failure analysis.

For the rest of the joints ($L_1$ = 20, 30, 40, and 50 mm) the value of critical longitudinal stresses (i.e., first pick value in the longitudinal stress variation along the bond length) were exported from elastic analyses. Furthermore, in order to better distinguish the numerical calculations behind the proposed failure prediction model, the longitudinal stress distribution along the path defined in the mid-plane of the adhesive layer for the other joints of the present experimental series has been depicted in Figures 6 and 7. The variation of critical longitudinal stresses for different bonding lengths are illustrated in Figure 8. As it is obvious, the bonding length of $L_1$ = 30 mm is the effective bonding length and for higher bonding lengths the longitudinal stress remains constant. To have more accurate prediction of the bonding length, higher numbers of finite element analyses on the DSJ models with the bonding length in the range of $L_1$ = 30 mm can be undertaken.
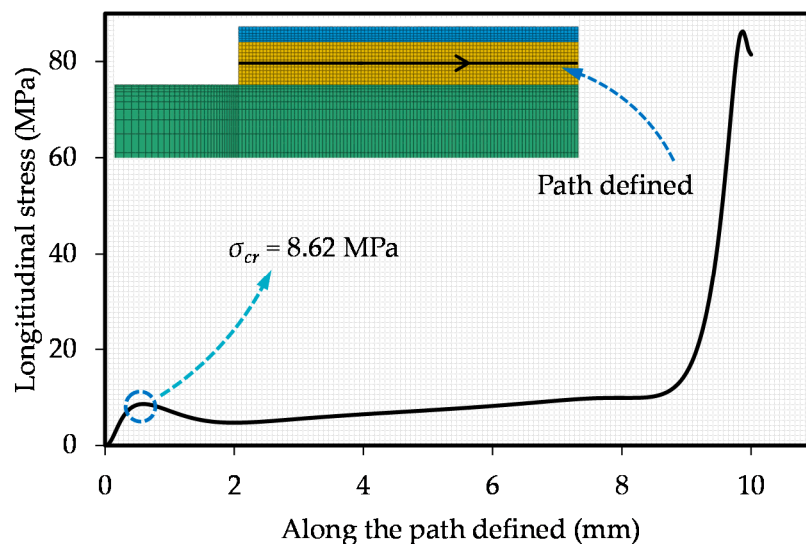


**Figure 6.** Longitudinal stress distribution along the path defined in the mid-plane of the adhesive layer for the present experimental series—$L_1$ = 10 mm.
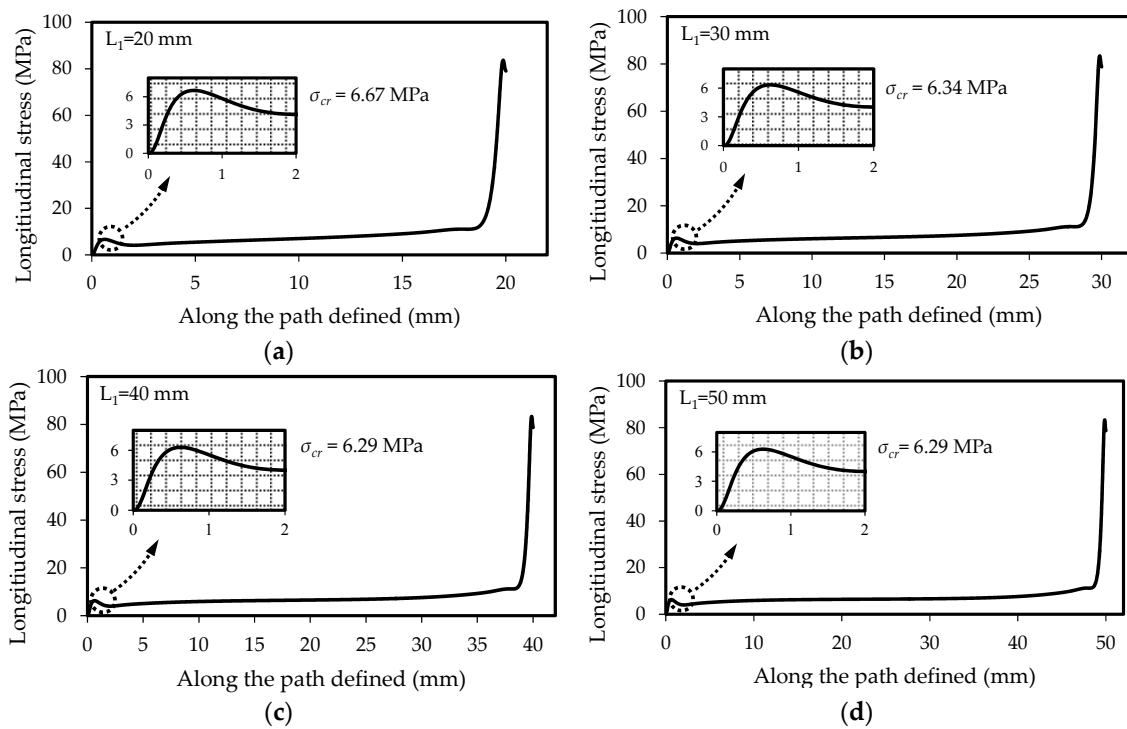
**Figure 7.** Longitudinal stress distribution along the path defined in the mid-plane of the adhesive layer for the present experimental series—(**a**) $L_1$ = 20 mm; (**b**) $L_1$ = 30 mm; (**c**) $L_1$ = 40 mm; (**d**) $L_1$ = 50 mm (applied stress for all the specimens: 1000 MPa).
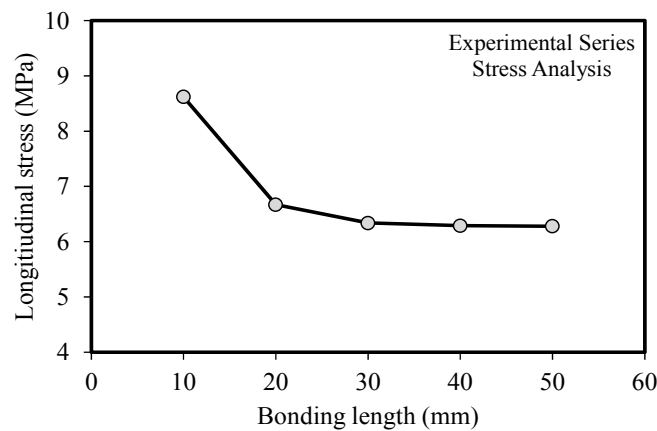


**Figure 8.** The variation of critical longitudinal stress for different bonding lengths (applied stress for all the specimens: 1000 MPa).

### 4.2. How to Obtain the Theoretical Failure Loads of the Double Strap Joint (DSJ) Specimens by Means of the PS Method

In order to obtain the failure loads of the joints the Equation (1) is proposed which includes a linear part for bonding lengths less than $L_{\text{eff}}$ and a constant part for DSJs with larger bonding lengths.

$$P_{\text{Theor.}} = \begin{cases} (0.8\frac{L_1}{L_{\text{eff}}} + 0.2)F^* & 0 < L_1 < L_{\text{eff}} \\ F^* & L_{\text{eff}} \leq L_1 \end{cases} \tag{1}$$

The parameter $F^*$ in Equation (1) is the experimental failure load of adhesive joints with bonding length higher than the effective bonding length. According to this method, by testing only one DSJ the failure loads of DSJs with different bonding lengths can be predicted. Considering any of the tested

DSJs with bonding lengths higher than $L_{\text{eff}}$ in previous sections as the reference joint for failure load prediction results in the theoretical predictions which are presented in Table 3 and Figure 9. Good agreement is seen between the PS predictions and the experimental results.

**Table 3.** Dimensions of the adhesive joints and details of experimental and theoretical failure loads for the tested DSJs.

| Bonding Length, $L_1$ | Bonding Length, $L_2$ | Experimental Failure Load, $P_{\text{Exp.}}$ (kN) | Theoretical Failure Load, $P_{\text{Theor.}}$ (kN) | $P_{\text{Theor.}}/P_{\text{Exp.}}$ |
|---|---|---|---|---|
| 10 | 40 | 13.33 | 14.67 | 1.10 |
| 20 | 50 | 24.36 | 23.05 | 0.95 |
| 30 | 60 | 31.43 | 31.43 | 1.00 |
| 40 | 70 | 30.17 | 31.43 | 1.04 |
| 50 | 80 | 31.93 | 31.43 | 0.98 |
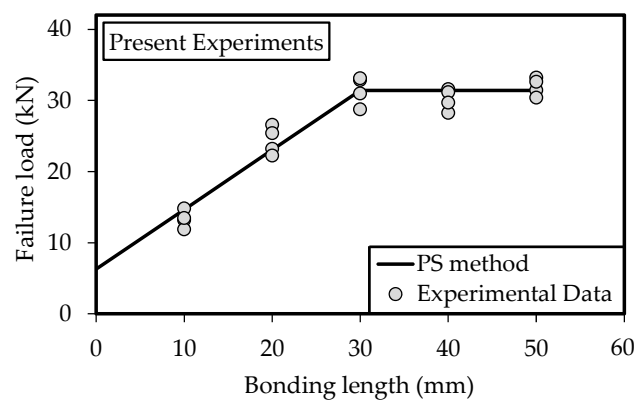


**Figure 9.** Comparison between the experimental failure loads of DSJs and the theoretical predictions obtained by means of point stress (PS) method.

For further validation, the proposed method was used to predict the failure loads of two series of DSJs which have been reported in previous experimental study by Al-Zubaidy et al. [26,28]. Al-Zubaidy et al. [26,28] conducted some experiments on DSJs of width 50 mm and bonding lengths of $L_1$ = 10, 20, 30, 40, 50, 60, 70, 80, 90, and 100 mm. The DSJs were made from 5 mm thick steel plates of 210 mm length, reinforced on both sides with unidirectional carbon fiber sheets. For the experimental data series A, one layer of CFRP sheet was bonded on each side of the joint. For the experimental data series B, three layers of CFRP sheets were bonded on each side of the adhesive joint. The Araldite 420 adhesive was used for joining the CFRP sheets together and also joining them to the steel plates. Each layer of CFRP had a thickness of 0.176 mm, while the thickness of the adhesive layer was 0.53 mm. For some geometry, three tests and for the other ones two tests have been performed by Al-Zubaidy et al. [26,28] to check the repeatability of the experimental results.

For the joints series B, three layers of CFRP were composed of two adhesive layers to produce a total thickness of 1.588 mm. Table 4 presents the mechanical properties of the tested joints. In order to simplify the numerical modelling, three layers of CFRP and two layers of adhesive between them in the joints series B were considered as one part having an equivalent tensile modulus which can be calculated from [21] as follows:

$$E_{\text{eq}} = \frac{E_{\text{adh}} \times t_{\text{adh}} + E_{\text{CFRP}} \times t_{\text{CFRP}}}{t_{\text{adh}} + t_{\text{CFRP}}} \tag{2}$$

in which $E_{\text{eq}}$ is the equivalent modulus of the CFRP/adhesive layer, and $E_{\text{adh}}$ and $E_{\text{CFRP}}$ are the tensile modulus of the adhesive layer and CFRP sheets, respectively. The terms $t_{\text{adh}}$ and $t_{\text{CFRP}}$ signify the total bond line thickness and the thickness of the CFRP layers. Details of the experimental failure loads are

listed in Table 5. $P_{\text{Exp}. i}$ ($i$ = 1, 2, 3) and $P_{\text{Exp}.}$ specify the failure loads of the three repeated tests and the average value of the three experimental failure loads, respectively.

A similar method was applied to obtain the effective bonding length $L_{\text{eff}}$ and predict the failure loads of all bonding lengths. Table 6 summarizes the values of the failure load, obtained experimentally from the tensile quasi-static tests on the DSJ specimens and numerically by means of the FE analyses based on the PS method, including the discrepancies.

Figure 10 shows the curves of critical longitudinal stresses as a function of bonding length for the joints series A and series B. According to the plateaus in Figure 10, the effective bonding lengths of the joints series A and B are 30 and 50 mm, respectively. Using these effective bonding lengths and considering one of the joints ($L_1 > L_{\text{eff}}$) as the reference joints, the failure loads of the remaining joints were estimated using the PS method. A comparison between the PS predictions and the experimental results is illustrated in Figure 11. Again, a very good correlation is seen between the experimental data and PS estimates for failure loads in the tested DSJs.

**Table 4.** Mechanical properties of materials used for joints series A and B [21,22].

| Property | Steel Plates | Adhesive | CFRP Sheets |
|---|---|---|---|
| Tensile modulus (GPa) | 200 | 1.9 | 240 |
| Equivalent tensile modulus for the joints series B (GPa) | - | - | 88.7 |
| Poisson's ratio | 0.25 | 0.21 | 0.28 |

**Table 5.** Summary of the test results reported by Al-Zubaidy et al., for the double strap joints series A and B [26,28].

| Specimen Label | Bonding Length, $L_1$ | Bonding Length, $L_2$ | $P_{\text{Exp.1}}$ (kN) | $P_{\text{Exp.2}}$ (kN) | $P_{\text{Exp.3}}$ (kN) | $P_{\text{Exp.}}$ (kN) (Standard Deviation) |
|---|---|---|---|---|---|---|
| A | 10 | 80 | 19.84 | - | - | 19.84 (-) |
| A | 20 | 80 | 35.61 | 40.14 | - | 37.87 (8%) |
| A | 30 | 80 | 46.16 | 44.27 | - | 45.22 (3%) |
| A | 40 | 80 | 46.40 | 41.73 | - | 44.06 (7%) |
| A | 50 | 80 | 45.97 | 48.91 | - | 47.44 (4%) |
| A | 60 | 80 | 45.92 | 46.43 | - | 46.17 (1%) |
| A | 70 | 100 | 43.99 | 48.67 | - | 46.33 (7%) |
| A | 80 | 100 | 50.13 | 46.23 | - | 48.18 (6%) |
| A | 90 | 115 | 46.97 | 44.68 | - | 45.82 (4%) |
| A | 100 | 115 | 47.28 | 46.19 | - | 46.73 (2%) |
| B | 10 | 80 | 29.61 | - | - | 29.61 (-) |
| B | 20 | 80 | 51.22 | 54.91 | 56.47 | 54.20 (5%) |
| B | 30 | 80 | 66.89 | 71.37 | 68.36 | 68.88 (3%) |
| B | 40 | 80 | 80.38 | 84.23 | 84.03 | 82.88 (3%) |
| B | 50 | 80 | 101.67 | 86.50 | 102.32 | 96.83 (9%) |
| B | 60 | 80 | 104.06 | 93.36 | 106.63 | 101.35 (7%) |
| B | 70 | 100 | 111.54 | 89.12 | 109.07 | 103.24 (12%) |
| B | 80 | 100 | 93.95 | 91.13 | 107.12 | 97.40 (9%) |
| B | 90 | 115 | 91.21 | 93.51 | 107.40 | 97.38 (9%) |
| B | 100 | 115 | 96.75 | 91.80 | 109.12 | 99.22 (9%) |

**Table 6.** Details of experimental results with theoretical failure load predictions for the joints series A and B.

| Specimen Label | Bonding Length, $L_1$ | Bonding Length, $L_2$ | Average of Experimental Failure Load, $P_{Exp.}$ (kN) [28] | Theoretical Failure Load, $P_{Theor.}$ (kN) | $P_{Theor.}/P_{Exp.}$ |
|---|---|---|---|---|---|
| A | 10 | 80 | 19.84 | 21.1 | 1.06 |
| A | 20 | 80 | 37.87 | 33.16 | 0.88 |
| A | 30 | 80 | 45.22 | 45.22 | 1 |
| A | 40 | 80 | 44.06 | 45.22 | 1.03 |
| A | 50 | 80 | 47.44 | 45.22 | 0.95 |
| A | 60 | 80 | 46.17 | 45.22 | 0.98 |
| A | 70 | 100 | 46.33 | 45.22 | 0.98 |
| A | 80 | 100 | 48.18 | 45.22 | 0.94 |
| A | 90 | 115 | 45.82 | 45.22 | 0.99 |
| A | 100 | 115 | 46.73 | 45.22 | 0.97 |
| B | 10 | 80 | 29.61 | 34.86 | 1.18 |
| B | 20 | 80 | 54.20 | 50.35 | 0.93 |
| B | 30 | 80 | 68.88 | 65.84 | 0.96 |
| B | 40 | 80 | 82.88 | 81.34 | 0.98 |
| B | 50 | 80 | 96.83 | 96.83 | 1 |
| B | 60 | 80 | 101.35 | 96.83 | 0.96 |
| B | 70 | 100 | 103.24 | 96.83 | 0.94 |
| B | 80 | 100 | 97.40 | 96.83 | 0.99 |
| B | 90 | 115 | 97.38 | 96.83 | 0.99 |
| B | 100 | 115 | 99.22 | 96.83 | 0.98 |
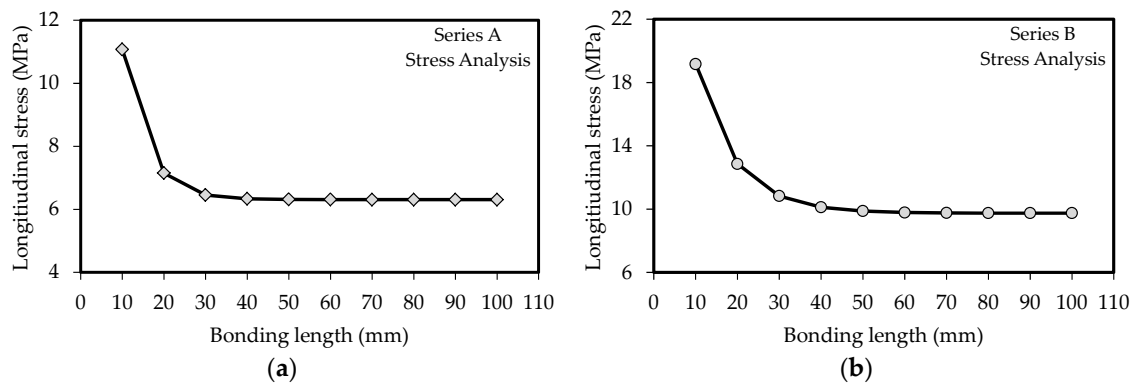


**Figure 10.** The variation of critical longitudinal stress for different bonding lengths (applied stress for all the specimens: 1000 MPa); (**a**) series A; (**b**) series B.
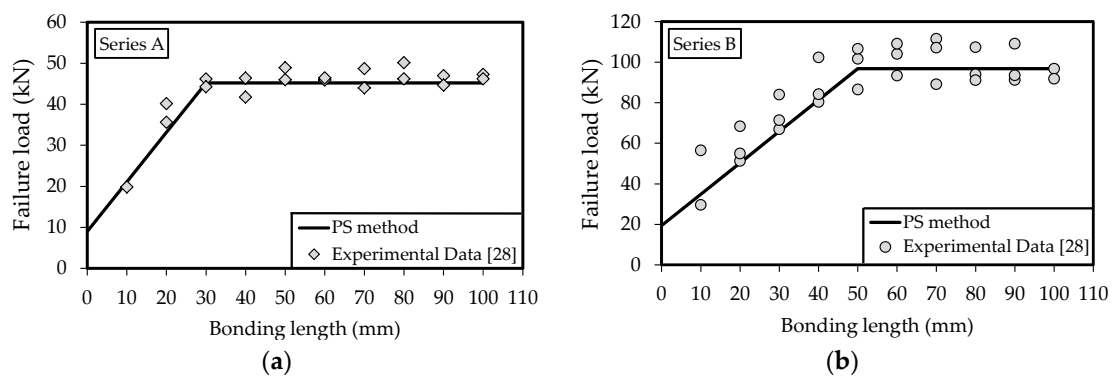


**Figure 11.** Comparison between the experimental failure loads of DSJs and the theoretical predictions obtained by means of PS method; (**a**) series A; (**b**) series B.

Different methods based on strain, stress, and energy have also been suggested in literature to predict the failure behavior of adhesively bonded joints (see Refs. [21–23,37–45]). They commonly require consideration of material nonlinear behavior in finite element simulation and need a higher number of material properties to estimate the failure loads of the adhesive joints. However, in the PS method failure can be easily predicted only by conducting 2D-linear elastic analyses. Comparing the current prediction results with previously published results available in the open literature reveals that the average accuracy of the point stress method is in the same order of the other failure models such as the cohesive zone model and the Hart–Smith model. Due to the advantages noted above, one may recommend the use of the PS method for predicting the failure load in steel/CFRP DSJs.

The same methodology can be applied to estimate the failure load in other metallic alloys and FRP materials which are investigated in some studies dealing with practical applications of FRP-reinforced and -retrofitted structures [46–52].

## 5. Failure Mechanisms in Steel/Carbon Fiber Reinforced Polymer (CFRP) DSJs

Six types of failure mechanisms exist in steel/CFRP DSJs under various loadings, including CFRP rupture (fiber breakage), debonding between the CFRP and the adhesive layer or between the steel plates and the adhesive layer (adhesive failure), failure in the adhesive layer (cohesive failure), CFRP delamination, and steel plate yielding. A schematic of these failure mechanisms for steel/CFRP DSJs have been illustrated in Figure 12.

Zhao and Zhang [33] have previously studied these failure mechanisms. More recently, different types of failure modes in steel/CFRP double strap joints have been investigated by Al-Mosawe et al. [30]. They studied the effect of failure modes in stress variations along the bonding length and compared these data with the results presented by Al-Zubaidy et al. [26]. Also shown in Figure 2b, fiber breakage (rupture in CFRP) predominantly occurred in the tested DSJs. For further failure assessment of steel/CFRP DSJs, the fracture surfaces of the tested specimens were investigated using optical microscopy. It was revealed that the majority of the failure is governed by CFRP rupture and CFRP delamination close to the junction of steel substrates. The optical microscopy pictures of adhesive fracture surfaces are shown in Figure 13. Additionally, the dominant failure modes in the tested DSJs in the experimental works reported in Ref. [28] were adhesive failure, CFRP delamination, CFRP rupture, and steel/adhesive interface debonding. It is worth mentioning that the PS method was able to predict the effective bonding length for DSJs which failed under various failure mechanisms, including interfacial debonding (adhesive failure), CFRP delamination, and CFRP rupture.
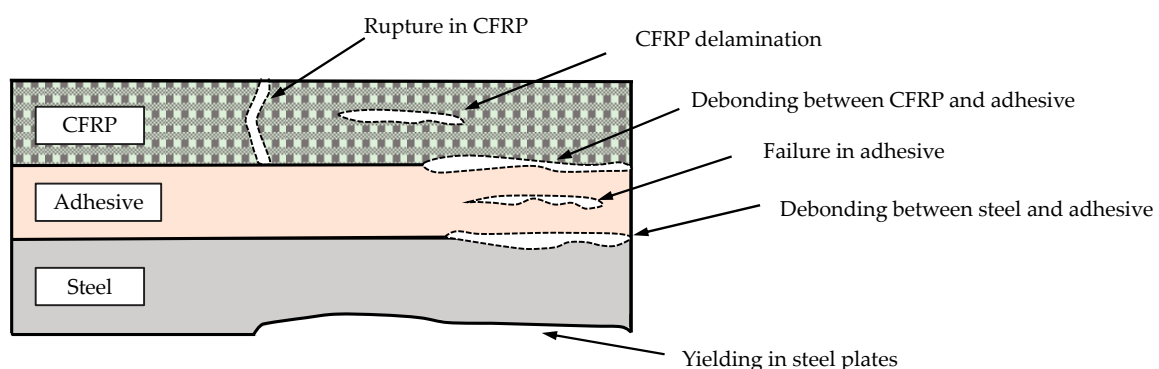


**Figure 12.** Different types of failure mechanisms in steel/CFRP bonded joint.
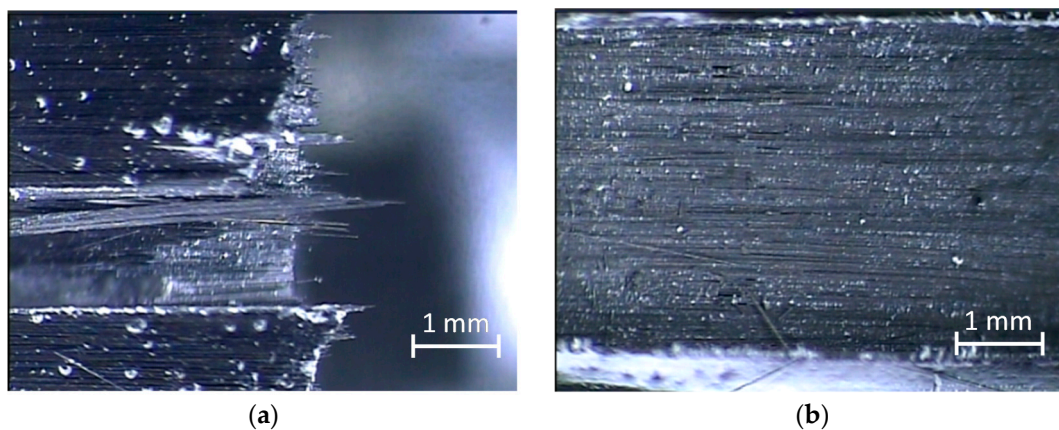
**Figure 13.** Typical failure mode of loaded steel/CFRP DSJs subjected to quasi-static tensile loading; (**a**) CFRP rupture; (**b**) CFRP delamination.

## 6. Assumptions, Limitations, and Advantages of the PS Method for DSJs

According to the experimental results, the load–displacement curves were linear up to final fracture which took place suddenly with no effective plastic deformation in the adhesive layer, meaning the adhesive and the adherents remained in linear elastic conditions. Therefore, it is expected that the linear elastic fracture mechanics (LEFM) assumption can be utilized for failure load prediction of the tested DSJs. In other words, the proposed failure model in this research is more suitable to be applied for the joints having predominantly elastic behavior up to the failure load, or joints having little plastic deformation.

There are some limitations and advantages in using the PS method for DSJs as a failure load prediction model which are briefly discussed in this section. Generally, the term "failure" in this theoretical prediction model for DSJs describes the state of total failure modes such as adhesive layer failure (cohesive failure), debonding between the CFRP and the adhesive layer or between the steel plates and the adhesive layer (adhesive failure), CFRP rupture, CFRP delamination, or a combination of modes. The failure load predictions for different failure mechanisms were in good agreement with the experimental results.

In order to predict the failure loads of DSJs with different bonding lengths, only one DSJ corresponding to the effective bonding length should be tested, which is realized as an advantage of the methodology. Hence, it is very important to note that although the PS method for DSJs has one experimental part, one can estimate conveniently and rapidly the value of the effective bond length by applying the PS method proposed in this research before conducting any experiments. However, in some experimental research (see for instance Refs. [28,30]) complicated numerical finite element analysis by considering the material nonlinear behavior should be conducted to find the effective bond length. In fact, the simple calculation in predicting the effective bond length is the substantial advantage in the PS method for DSJs. Due to the advantages mentioned above, the efficiency of the PS method for predicting the failure load in the steel/CFRP DSJs has been demonstrated.

## 7. Conclusions

Use of CFRP materials as externally bonded sheets is one of the effective approaches to repair and improve the strength of the damaged steel structures. In this paper, a new method, namely the point stress method, was presented for failure load prediction in steel/CFRP adhesively bonded DSJs based on longitudinal stress along the adhesive mid-plane. According to this method, by calculation of the effective bonding length, the failure of DSJs with different bonding lengths can be predicted. Some experimental tests were conducted on DSJs and the results of theoretical predictions were compared with the experimental results. It was revealed that the average accuracy of the PS method

was very good and this method could estimate the experimental failure loads very well. The same methodology was applied to two sets of experimental results available in the literature and the failure loads of steel/CFRP DSJs with different bonding lengths were successfully predicted by means of the PS method.

## References

1. Ahmad, F.; Hong, J.W.; Choi, H.S.; Park, M.K. Hygro effects on the low-velocity impact behavior of unidirectional CFRP composite plates for aircraft applications. *Compos. Struct.* **2016**, *135*, 276–285. [CrossRef]

2. Carpinteri, A.; Cornetti, P.; Pugno, N. Debonding in FRP Strengthened Beams: Stress Assessment Versus Fracture Mechanics Approach. In Proceedings of the 6th Conference on Fracture Mechanics of Concrete and Concrete Structures (FraMCoS), Catania, Italy, 17–22 June 2007; pp. 1053–1060.

3. Colombi, P. Reinforcement delamination of metallic beams strengthened by FRP strips: Fracture mechanics based approach. *Eng. Fract. Mech.* **2006**, *73*, 1980–1995. [CrossRef]

4. Lenwari, A.; Thepchatri, T.; Watanabe, E. Prediction of premature separation of bonded CFRP plates from strengthened steel beams using a fracture criterion. *Struct. Eng. Mech.* **2002**, *14*, 565–574. [CrossRef]

5. Martiny, P.; Lani, F.; Kinloch, A.J.; Pardoen, T. A maximum stress at a distance criterion for the prediction of crack propagation in adhesively-bonded joints. *Eng. Fract. Mech.* **2013**, *97*, 105–135. [CrossRef]

6. Tong, L. Strength of adhesively bonded single-lap and lap-shear joints. *Int. J. Solids Struct.* **1998**, *35*, 2601–2616. [CrossRef]

7. De Morais, A.B.; Pereira, A.B.; Teixeira, J.P.; Cavaleiro, N.C. Strength of epoxy adhesive-bonded stainless-steel joints. *Int. J. Adhes. Adhes.* **2007**, *27*, 679–686. [CrossRef]

8. Karachalios, E.F.; Adams, R.D.; da Silva, L.F.M. Single lap joints loaded in tension with high strength steel adherends. *Int. J. Adhes. Adhes.* **2013**, *43*, 81–95. [CrossRef]

9. Khoramishad, H.; Razavi, S.M.J. Metallic fiber-reinforced adhesively bonded joints. *Int. J. Adhes. Adhes.* **2014**, *55*, 114–122. [CrossRef]

10. Nemati Giv, A.; Ayatollahi, M.R.; Razavi, S.M.J.; Khoramishad, H. The Effect of orientations of metal macrofiber reinforcements on mechanical properties of adhesively bonded single lap joints. *J. Adhes.* **2017**, 1–21. [CrossRef]

11. Esmaeili, E.; Razavi, S.M.J.; Bayat, M.; Berto, F. Flexural behavior of metallic fiber-reinforced adhesively bonded single lap joints. *J. Adhes.* **2017**, 1–20. [CrossRef]

12. Hart-Smith, L.J. *Adhesive-Bonded Single-Lap Joints*; Langley Research Center: Hampton, VA, USA, 1973.

13. Da Silva, L.F.; das Neves, P.J.; Adams, R.D.; Spelt, J.K. Analytical models of adhesively bonded joints—Part I: Literature survey. *Int. J. Adhes. Adhes.* **2009**, *29*, 319–330. [CrossRef]

14. Da Silva, L.F.; das Neves, P.J.; Adams, R.D.; Wang, A.; Spelt, J.K. Analytical models of adhesively bonded joints—Part II: Comparative study. *Int. J. Adhes. Adhes.* **2009**, *29*, 331–341. [CrossRef]

15. John, S.; Kinloch, A.; Matthews, F. Measuring and predicting the durability of bonded carbon fibre/epoxy composite joints. *Composites* **1991**, *22*, 121–127. [CrossRef]

16. Adams, R.; Peppiatt, N. Stress analysis of adhesive bonded tubular lap joints. *J. Adhes.* **1977**, *9*, 1–18. [CrossRef]

17. Lee, S.J.; Lee, D.G. Development of a failure model for the adhesively bonded tubular single lap joint. *J. Adhes.* **1992**, *40*, 1–14. [CrossRef]

18. Chen, Z.; Adams, R.D.; da Silva, L.F.M. Prediction of crack initiation and propagation of adhesive lap joints using an energy failure criterion. *Eng. Fract. Mech.* **2011**, *78*, 990–1007. [CrossRef]

19. Chalkley, P.; Rose, F. Stress analysis of double-strap bonded joints using a variational method. *Int. J. Adhes. Adhes.* **2001**, *21*, 241–247. [CrossRef]

20. Bocciarelli, M.; Colombi, P.; Fava, G.; Poggi, C. Prediction of debonding strength of tensile steel/CFRP joints using fracture mechanics and stress based criteria. *Eng. Fract. Mech.* **2009**, *76*, 299–313. [CrossRef]

21. Fawzia, S.; Al-Mahaidi, R.; Zhao, X.L. Experimental and finite element analysis of a double strap joint between steel plates and normal modulus CFRP. *Compos. Struct.* **2006**, *75*, 156–162. [CrossRef]

22. Fawzia, S.; Zhao, X.L.; Al-Mahaidi, R. Bond—Slip models for double strap joints strengthened by CFRP. *Compos. Struct.* **2010**, *92*, 2137–2145. [CrossRef]

23. Al-Shawaf, A. Modelling wet lay-up CFRP—Steel bond failures at extreme temperatures using stress-based approach. *Int. J. Adhes. Adhes.* **2011**, *31*, 416–428. [CrossRef]

24. Nguyen, T.C.; Bai, Y.; Zhao, X.L.; Bambach, M.R.; Al-Mahaidi, R. Temperature Effect on Adhesively Bonded CFRP and Steel Double Strap Joints. *Adv. FRP Compos. Civ. Eng.* **2011**, 877–880.

25. Nguyen, T.C.; Bai, Y.; Zhao, X.L.; Al-Mahaidi, R. Mechanical characterization of steel/CFRP double strap joints at elevated temperatures. *Compos. Struct.* **2011**, *93*, 1604–1612. [CrossRef]

26. Al-Zubaidy, H.A.; Zhao, X.L.; Al-Mahaidi, R. Dynamic bond strength between CFRP sheet and steel. *Compos. Struct.* **2012**, *94*, 3258–3270. [CrossRef]

27. Nguyen, T.C.; Bai, Y.; Zhao, X.L.; Al-Mahaidi, R. Effects of ultraviolet radiation and associated elevated temperature on mechanical performance of steel/CFRP double strap joints. *Compos. Struct.* **2012**, *94*, 3563–3573. [CrossRef]

28. Al-Zubaidy, H.A.; Al-Mahaidi, R.; Zhao, X.L. Finite element modelling of CFRP/steel double strap joints subjected to dynamic tensile loadings. *Compos. Struct.* **2013**, *99*, 48–61. [CrossRef]

29. Nguyen, T.C.; Bai, Y.; Zhao, X.L.; Al-Mahaidi, R. Curing effects on steel/CFRP double strap joints under combined mechanical load, temperature and humidity. *Constr. Build. Mater.* **2013**, *40*, 899–907. [CrossRef]

30. Al-Mosawe, A.; Al-Mahaidi, R.; Zhao, X.L. Effect of CFRP properties, on the bond characteristics between steel and CFRP laminate under quasi-static loading. *Constr. Build. Mater.* **2015**, *98*, 489–501. [CrossRef]

31. Al-Mosawe, A.; Al-Mahaidi, R.; Zhao, X.L. Bond behaviour between CFRP laminates and steel members under different loading rates. *Compos. Struct.* **2016**, *148*, 236–251. [CrossRef]

32. Majidi, H.R.; Razavi, S.M.J.; Ayatollahi, M.R. Failure load prediction of steel-CFRP double strap joints under quasi-static tensile loading. In Proceedings of the 5th International Conference on Composites: Characterization, Fabrication and Application (CCFA-5), Tehran, Iran, 20–21 December 2016.

33. Zhao, X.L.; Zhang, L. State-of-the-art review on FRP strengthened steel structures. *Eng. Struct.* **2007**, *29*, 1808–1823. [CrossRef]

34. Mohee, F.M.; Al-Mayah, A.; Plumtree, A. Anchors for CFRP plates: State-of-the-art review and future potential. *Compos. B Eng.* **2016**, *90*, 432–442. [CrossRef]

35. ASTM E8/E8M-16a. *Standard Test Methods for Tension Testing of Metallic Materials*; ASTM International: West Conshohocken, PA, USA, 2016; Available online: www.astm.org (access on 6 July 2017).

36. ASTM. *Properties, Standard Test Method for Tensile Properties of Plastics*; American Society for Testing and Materials: West Conshohocken, PA, USA, 1996.

37. Sato, C.; Ikegami, K. Tensile strength of single lap joint and scarf joint between CFRP and carbon steel. *J. Adhes.* **1992**, *39*, 29–41. [CrossRef]

38. Li, J.; Yan, Y.; Liang, Z.; Zhang, T. Experimental and Numerical Study of Adhesively Bonded CFRP Scarf-Lap Joints Subjected to Tensile Loads. *J. Adhes.* **2016**, *92*, 1–17. [CrossRef]

39. Razavi, S.M.J.; Esmaeili, E.; Samari, M.; Razavi, S.M.R. Stress analysis on a non-flat zigzag interface bonded joint. *J. Adhes.* **2016**, 1–19. [CrossRef]

40. Ayatollahi, M.R.; Nemati Giv, A.; Razavi, S.M.J.; Khoramishad, H. Mechanical properties of adhesively single lap-bonded joints reinforced with multi-walled carbon nanotubes and silica nanoparticles. *J. Adhes.* **2016**, 1–18. [CrossRef]

41. Razavi, S.M.J.; Ayatollahi, M.R.; Esmaeili, E.; da Silva, L.F.M. Mixed mode fracture response of a metallic fiber-reinforced epoxy adhesive. *Eur. J. Mech. A-Solids* **2017**, *65*, 349–359. [CrossRef]

42. Enghardt, S.; Richter, G.; Richter, E.; Reitemeier, B.; Walter, M.H. Experimental Investigations on the Influence of Adhesive Oxides on the Metal-Ceramic Bond. *Metals* **2015**, *5*, 119–130. [CrossRef]

43. Razavi, S.M.J.; Berto, F.; Peron, M.; Torgersen, J. Parametric study of adhesive joints with non-flat sinusoid interfaces. *Theor. Appl. Fract. Mech.* **2017**. [CrossRef]

44. Al-Mosawe, A.; Al-Mahaidi, R.; Zhao, X.L. Experimental and Numerical Study on Strengthening of Steel Members Subjected to Impact Loading Using Ultrahigh Modulus CFRP. *J. Compos. Constr.* **2016**, *20*, 04016044. [CrossRef]

45. Al-Mosawe, A.; Kalfat, R.; Al-Mahaidi, R. Strength of CFRP-steel double strap joints under impact loads using genetic programming. *Compos. Struct.* **2017**, *160*, 1205–1211. [CrossRef]

46. Ghafoori, E.; Motavalli, M. Flexural and interfacial behavior of metallic beams strengthened by prestressed bonded plates. *Compos. Struct.* **2013**, *101*, 22–34. [CrossRef]

47. Ghafoori, E. Interfacial stresses in beams strengthened with bonded prestressed plates. *Eng. Struct.* **2013**, *46*, 508–510. [CrossRef]

48. Ghafoori, E.; Motavalli, M. Lateral-torsional buckling of steel I-beams retrofitted by bonded and un-bonded CFRP laminates with different pre-stress levels: Experimental and numerical study. *Constr. Build. Mater.* **2015**, *76*, 194–206. [CrossRef]

49. Ghafoori, E.; Motavalli, M. Normal, high and ultra-high modulus CFRP laminates for bonded and un-bonded strengthening of steel beams. *Mater. Des.* **2015**, *67*, 232–243. [CrossRef]

50. Ghafoori, E.; Motavalli, M.; Botsis, J.; Herwig, A.; Galli, M. Fatigue strengthening of damaged metallic beams using prestressed unbonded and bonded CFRP plates. *Int. J. Fatigue* **2012**, *44*, 303–315. [CrossRef]

51. Ghafoori, E.; Motavalli, M.; Nussbaumer, A.; Herwig, A.; Prinz, G.S.; Fontana, M. Design criterion for fatigue strengthening of riveted beams in a 120-year-old railway metallic bridge using pre-stressed CFRP plates. *Compos. B Eng.* **2015**, *68*, 1–13. [CrossRef]

52. Ghafoori, E.; Prinz, G.S.; Mayor, E.; Nussbaumer, A.; Motavalli, M.; Herwig, A.; Fontana, M. Finite element analysis for fatigue damage reduction in metallic riveted bridges using pre-stressed CFRP plates. *Polymers* **2014**, *6*, 1096–1118. [CrossRef]